Ceramics-Silikáty 66 (3), 280-288 (2021)
www.ceramics-silikaty.cz doi: 10.13168/cs.2022.0024

HYDRATION CHARACTERISTICS AND EXPANSION BEHAVIOUR OF PORTLAND CEMENT WITH B-DOPED MgO

HE XUAN*, #HUANG LEI*,**, WU CHENGYOU*,**, HUANG ZHENGYI*

*Department of Civil Engineering, Qinghai University, Xining 810016, China
**Qinghai Provincial Key Laboratory of Energy-saving Building Materials and Engineering Safety, Xining 810016, China

#E-mail: leihyx@foxmail.com

Submitted April 3, 2022; accepted May 20, 2022

Keywords: MgO expansion agent, B-impurity, Expansion rate, Hydration process, Compressive strength

The work focuses on a study of the hydration characteristics and expansion behaviour of Portland cement with B-doped MgO at an early age. The B-doped MgO was prepared from the co-calcination of a magnesium hydroxide reagent and a mixture of magnesium hydroxide and boric acid at 800 °C. The hydration process, products, and the porosity of pastes were investigated. Meanwhile, the physical and mechanical properties of the mortars were also determined. The results show that the co-calcination of B and magnesium at 800 °C changes the characteristics of the MgO crystals and their activity. With an increase in the dosage of B, the dimensions of the MgO crystals become smaller, and the specific surface area increases, but the activity decreases. The mortars with B-doped MgO show a higher expansion rate. The incorporation of B-doped MgO alters the hydration process of the cement pastes; 4 % B-doped MgO incorporation leads to the most increased cumulative heat at 120 h. The content of $Mg(OH)_2$ formed in the sample is the highest compared to that of the others. The initial setting time of cement paste is delayed by incorporating B-doped MgO. The higher the dosage of B, the later the initial setting time. The B-doped MgO incorporation increases the compressive strength of the cement pastes at 3 days, but significantly decreases at 28 days.

INTRODUCTION

Shrinkage cracking has always been an unavoidable technical problem for concrete materials. However, in recent years, due to the change in the quality of concrete raw materials, the improvement in the strength, the pumping construction of large flow concrete, and the complexity of structural forms, the cracking risk of modern concrete structures has been significantly increased [1]. In this regard, engineers and researchers have adopted various means to reduce the cracking risks of concrete. A concrete expansion agent to prepare shrinkage compensating concrete is a widely used method. The MgO expansion agent (MEA) has the advantages of stable hydration products, adjustable expansion performance, and compensates for the later shrinkage of concrete [2]. Therefore, it is gradually being recognised by more and more researchers and engineers and applied to important projects.

At present, MEA is mainly obtained by the calcination of magnesite [3]; due to the wide applications of magnesite in the industrial field, MEA obtained by magnesite is much more expensive. Therefore, many researchers have sought for substitutes to prepare MEA. In consideration of the compositions, dolomite ($CaMg(CO_3)_2$) was thought to be an ideal substitute. However, it was found that the expansion ability of MEA calcined by dolomite was poor, resulting from the effect of the existing calcium in dolomite. Temiz et al. [4] attempted to use blast furnace slag to consume calcium oxide to eliminate its adverse effect, but the result was negative. Xu [5] and Gao et al. [6, 7] put serpentine ($Mg_6[Si_4O_{10}](OH)_8$) together with dolomite to calcine MEA; the obtained MEA can effectively compensate for early shrinkage, but is prone to expansion and cracking at a later age.

Salt lakes in China are rich in magnesium resources. According to statistics, the magnesium salt reservoir is about 4.816 billion tonnes in salt-lake brine [8]; with the development of magnesium resources in salt lakes, a large amount of by-products containing magnesium can be produced. The lithium extraction industry produces a large amount of magnesium slag (MS), mainly composed of $Mg(OH)_2$. Besides, MS also contains a small amount of B, Li, K, Na, etc. Some researchers have attempted to utilise MS in building materials. Tan [9] and Dong [10] studied the characteristics of calcined MS under different calcination conditions and the properties of a potassium magnesium phosphate cement produced with MS. It was found that the main components of the calcined magnesium slag were MgO and $Mg_3B_2O_6$. The higher the calcination temperature is, the larger the par-

ticle size is. The setting of the potassium magnesium phosphate cement was delayed, and a low calcination temperature decreased the early compressive strength of the cement. Li [11] found that the coexisting elements in MS, including B, Li, etc. could help to sinter MS and, therefore, affect the setting behaviour and mechanical properties of the cement made with MS. Wu [12] produced basic magnesium sulfate cement with MS and pointed out that the coexisting elements in MS had significant effects on the cement hydration process and mechanical properties.

The by-product of the lithium extraction industry—MS, is an ideal substitute for magnesite to produce MEA. However, due to the high cost in the purification process, it is impractical to remove impurities in MS. Thus, it is critical to discover the effects of the impurities existing in MS on the MEA properties. Therefore, this study explores the influence of B, the main impurity existing in MS, on the crystallisation characteristics and the hydration activity of calcined MgO. Meanwhile, the hydration process, expansion behaviour, and mechanical properties of cement with B-doped MgO were also considered. Therefore, this study can provide theoretical guidance and reference for preparing MEA from MS containing impurities in salt lakes as well as the application of the MEA in engineering projects.

EXPERIMENTAL

Raw materials

The chemical composition of the Portland cement used in the study is shown in Table 1. An analytical pure magnesium hydroxide ($Mg(OH)_2$) reagent and an analytical pure boric acid (H_3BO_3) reagent were used for the calcination of B-doped MgO and ISO (International Organization for Standardization) standard sand was used for the preparation of the mortars.

Table 1. Chemical composition (%).

Composition	CaO	SiO_2	Fe_2O_3	MgO	Al_2O_3	SO_3	K_2O	Na_2O
Cement	68.7	16.8	3.4	1.7	4.3	3.2	0.6	0.2

Sample Preparation

The MgO and B-doped MgO were obtained by calcining the magnesium hydroxide reagent and the mixture of magnesium hydroxide and boric acid. The mix proportions are shown in Table 2. The reagents were well mixed and placed into alumina crucibles, and then the crucibles were put into a muffle furnace (GWL-1200 °C) and heated at the rate of 5 °C·min^{-1}; when the temperature reached 800 °C, the muffle furnace was set as an isothermal model and lasted for 2 hours. Afterward, the muffle furnace was shut down, and the specimens were cooled to room temperature in the muffle furnace chamber.

Table 2. Mix proportions of the calcined MgO (%).

Samples	Magnesium hydroxide	Boric acid
M0B	100	0
M4B	96	4
M8B	92	8

The mix proportions of the mortars are shown in Table 3; the mortar samples were prepared according to Chinese standard GB/T 17671, with a water/binder ratio of 0.5 and a sand/binder ratio of 3. The prepared mortar samples were cured at 20 °C ± 2 °C and 95 ± 5 % relative humidity. The demoulding was conducted after 3 d; afterward, the mortars were cured until the scheduled ages.

Table 3. Mix proportions of the mortars (g).

Samples	Cement	MgO			Standard sand	Water
		M0B	M4B	M8B		
MC	450				1350	225
MM0B	423	27			1350	225
MM4B	423		27		1350	225
MM8B	423			27	1350	225

The mixed proportions of the cement pastes are shown in Table 4. After mixing, the pastes were cast into sealed containers and cured at 20 °C. When it comes to the scheduled age, the pastes were immersed in ethanol for 12 h to stop the hydration; then, the pastes were dried for testing.

Table 4. Mix proportions of the cement pastes.

Samples	Cement (%)	MgO (%)			W/C
		M0B	M4B	M8B	
PC	100				0.5
PM0B	94	6			0.5
PM4B	94		6		0.5
PM8B	94			6	0.5

Test method

The lengths of the mortars were tested by a comparator, and the compressive strength of the cement pastes was tested at the scheduled ages. In addition, the initial setting time of the cement was tested by a Vicat apparatus. The water requirement for the cement pastes to obtain its normal consistency was firstly tested

according to the Chinese standard GB/T 1346. The initial setting time of pastes was determined when the penetration depth of the Vicat needle was 36 ± 1 mm.

An isothermal calorimeter (Calmetrix-4000HPC) was adopted to monitor the hydration heat evolution of the cement pastes prepared according to Table 4. The record was continuously conducted for 120 h. Before testing, the calorimeter was equilibrated at 20 °C for 12 h.

A Scanning Electron Microscope was used to observe the crystal morphology of the calcined MgO (su-8000, Hitachi, Tokyo, Japan). The X-Ray Diffraction (XRD) patterns of the calcined MgO and the dried cement pastes were collected by an X-ray diffractometer (D/max-2500pc, RIGAKU, Tokyo, Japan) at an accelerating voltage of 30 kV. The 2θ range was from 5° to 85° for the calcined MgO and from 5° to 65° for the cement pastes. The scanning speed was maintained at 6° per minute. A thermal gravimetric analyser (HCT-1, HENVE, Beijing, China) was used to determine the ther-mal properties of the samples, where the heating rate was 5 °C·min^{-1}, and the samples were heated from 30 °C to 1050 °C. The pore structure of the samples was measured through the mercury intrusion porosimetry (MIP) method with an automatic mercury porosimeter (AutoPore IV 9500, Micromeritics, Norcross, Georgia, USA).

RESULTS AND DISCUSSION

Characteristics of the B-doped MgO

Figure 1 shows the XRD patterns of M0B, M4B, and M8B. There are no other diffraction peaks other than MgO for M0B and M4B, whereas the incorporation of 8 % H_3BO_3 leads to the formation of $Mg_3B_2O_6$, shown in the XRD patterns of M8B. Therefore, in addition to the crystal compositions, incorporating H_3BO_3 (both M4B and M8B) changes the height and width of the MgO diffraction peaks compared to M0B, meaning that the crystal morphology of the MgO is influenced by the H_3BO_3 incorporation during the calcination process. To figure out the effect of B on the crystal morphology of MgO, the crystal dimensions of MgO were calculated based on the Scherrer equation (Equation 1) [13]. Moreover, the specific surface area based on the Brunauer-Emmett-Teller (BET) method and activity of the MgO based on the time required for citric acid colour change were tested, and all are shown in Table 5.

$$D = \frac{K\gamma}{B\cos\theta} \quad (1)$$

where K is Scherrer's constant, D is the average thickness of the grain perpendicular to the crystal surface, B is the half-height width of the measured sample diffraction peak, θ is the diffraction angle, and γ is the X-ray wavelength, which is 0.154 nm.

As shown in Table 5, the crystal size of the B-doped MgO is smaller than that of the pure MgO. Accordingly, the BET surface area increased by 17.94 $m^2 \cdot g^{-1}$ and 3.65 $m^2 \cdot g^{-1}$ for M4B and M8B, respectively, indicating that the degree of crystallisation of the pure MgO is higher than that of the B-doped MgO. However, compared to M0B, the citric acid colour time for M4B and M8B are extended by 7 s and 15 s, respectively, which seems contradictory to the variations in the crystal size and BET surface area.

Table 5. Properties of the MgO obtained by calcination at 800 °C.

Sample	Crystallite dimension (nm)	BET surface area ($m^2 \cdot g^{-1}$)	Citric acid colour change time (s)
M0B	19.27	30.14	38
M4B	13.84	48.08	45
M8B	15.39	33.79	53

The morphologies of the calcined MgO are shown in Figure 2. Tiny pits were found everywhere on the surface of crystalline grains for M0B. The pits on the

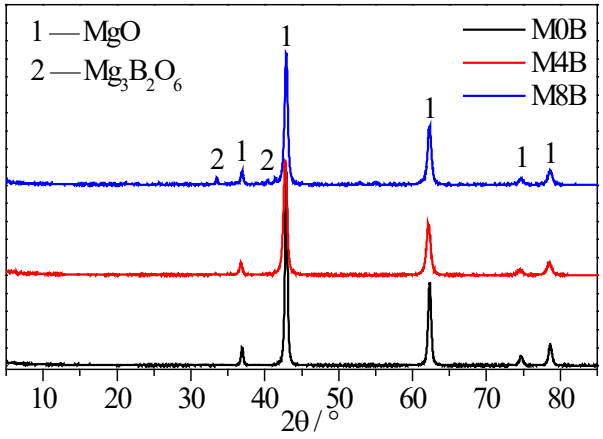

Figure 1. XRD patterns of the MgO calcined at 800 °C.

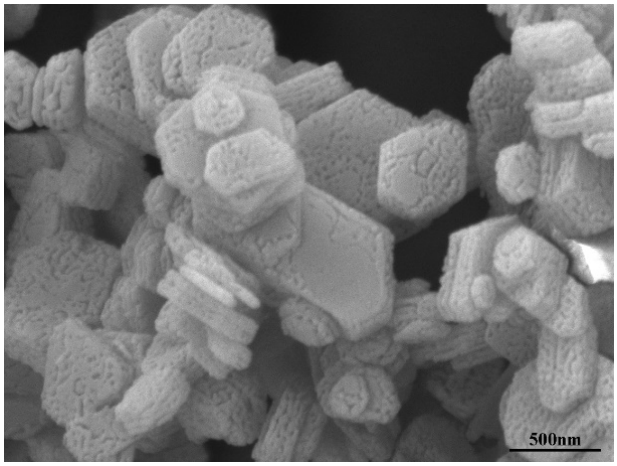

a) M0B

Figure 2. Morphologies of the calcined MgO.

continue on the next page ...

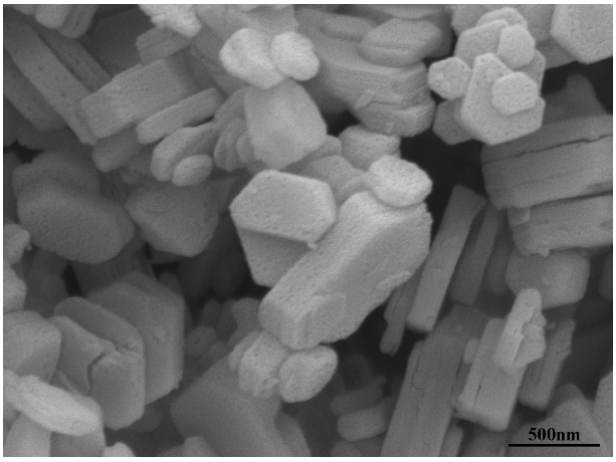

b) M4B

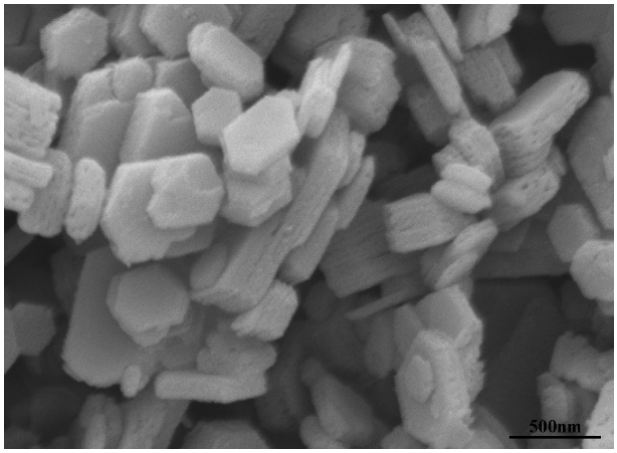

c) M8B

Figure 2. Morphologies of the calcined MgO.

surface of M4B became sparser and shallower than M0B and are hardly found on the surface of M8B. Then, it is understandable that M0B, which has a larger crystal size and a smaller BET surface than that of the B-doped MgO, shows a higher reactive activity (shown as a shorter citric acid colour time). Based on the dissolution theory [14], the formation of etch pits on the surface of the crystals is the critical step in the dissolution process. The more the etch pits formed, the easier the crystals dissolved. Thus, the preformed pits on the surface of M0B during the calcination process are helpful to its dissolution, thus, presenting with the higher reactive activity.

Expansion

Figure 3 shows the free expansion rate of the mortars. All the samples expand before the age of 3 d. Afterward, the mortars without the MgO incorporation begin to shrink, and the other samples continue to expand. Among the samples with the MgO incorporation, the expansion rate of MM0B is the lowest, and its expansion tends to be stable at an earlier age compared to MM4B and MM8B. The expansion speed of MM4B is the highest at an early age, whose expansion rate is the highest. When the age reaches 28 d, the shrinkage rate of MC is 0.013, whereas the expansion rates of MM0B, MM4B, and MM8B are 0.016, 0.034, and 0.030, respectively. Afterward, the expansion speed of MM8B is markedly accelerated. When the age reaches 60 d, the expansion rate of MM8B exceeds that of MM4B.

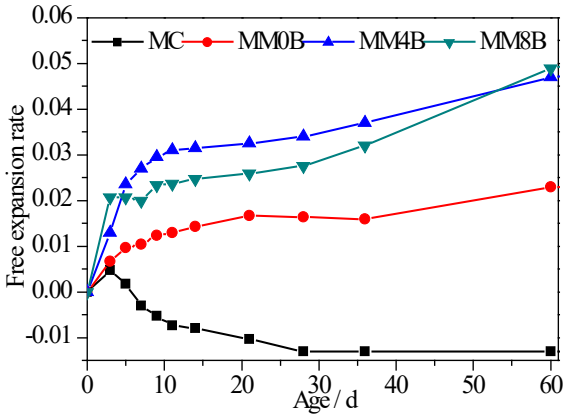

Figure 3. Free expansion rate of the mortars.

The expansion behaviour of MEA is significantly influenced by its reactivity [15], which determines the start and end time of the expansion, the expansion speed, and the final expansion rate. The expansion behaviours of MM4B and MM8B are consistent with the B-doped MgO's reactivity. The higher the reactivity of MgO, the lower the expansion speed and the higher the final expansion rate. Both the expansion speed and the expansion rate of MM0B are the lowest compared to MM4B and MM8B, which might result from the extremely high reactivity of M0B. Due to the high reactivity, the hydration of MgO is significantly advanced and might occur before the hardening of the cement, so the growth of $Mg(OH)_2$ makes little contribution to the volume change of the mortars. In addition to the reactivity effect, the expansion behaviour of the mortars might also be affected by the B dissolved in the pore solution.

Hydration process

The exothermic rate of the cement pastes with the B-doped MgO is shown in Figure 4a. It can be seen that the incorporations of MgO promotes the hydration process of the cement pastes, and the induction period length of PM0B, PM4B, and PM8B are shortened. Moreover, the incorporation of MgO significantly increases the height of the main exothermic peak. Compared to PC, the size of PM0B, PM4B, and PM8B are increased by 2.38 $mW \cdot g^{-1}$, 1.72 $mW \cdot g^{-1}$, and 1.95 $mW \cdot g^{-1}$, respectively. Furthermore, the dosage of the B-doped MgO affects the samples' hydration; compared to PM0B, the time the maximum exothermic peak

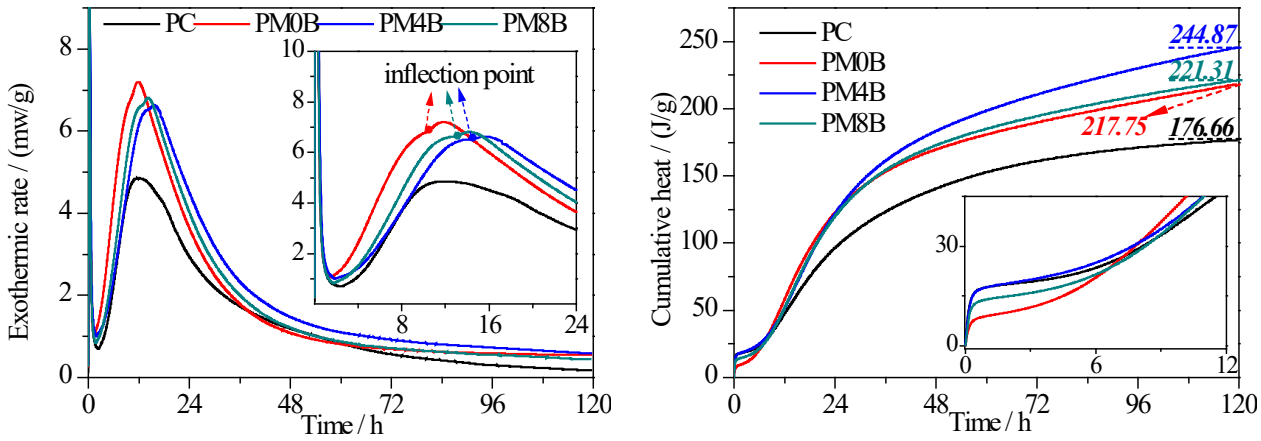

Figure 4. Exothermic rate and cumulative heat release of the cement pastes with the B-doped MgO.

occurs is delayed by 4.12 h and 2.28 h, respectively when 4 % and 8 % B were doped in the MgO. In addition to the differences in the exothermic rate, the cumulative heat of the pastes is prominently affected by the MgO incorporation. As shown in Figure 4b, the effect exerted by the MgO incorporation is different with an increase in the curing age. Before the age of 10 h, the heat release is suppressed by the MgO incorporation. Among the samples with the MgO incorporation, the sample with the 4 % B-doped MgO has the maximum heat release. Afterward, the effect exerted by the MgO incorporation on the heat release turns into promotion. When the age reaches 120 h, the cumulative heat of PM0B, PM4B, and PM8B are increased by 41.06 $J \cdot g^{-1}$, 68.21 $J \cdot g^{-1}$, and 44.65 $J \cdot g^{-1}$, respectively, compared to PC.

The shortening induction of the samples with the MgO incorporation could be attributed to the differences in the hydration activity between MgO and C3S (the main hydration mineral phase of cement at an early age). Because the hydration activity of MgO is lower than C3S, more water could be supplied to the reaction with C3S in the samples with the MgO incorporation at an early age. As a result, the dissolution of C3S is accelerated, and a larger C-S-H nucleus is accumulated. Therefore, the induction is shortened. The larger the C-S-H nucleus that accumulates more sites and space for C-S-H growth are provided, resulting in a faster growth rate, shown as the higher main exothermic peaks for the samples with the MgO incorporation in Figure 4a. In addition to the alteration in the hydration exothermic rate, the incorporation of MgO also leads to the inflection in the exothermic rate curves, and it results from the hydration of MgO.

The dopant of B in MgO alters the crystallisation characteristics and reduces the hydration activity of MgO. Thus, it could be anticipated that the sample with B-doped MgO has a higher exothermic rate, considering the effect of the hydration activity of the additions on the exothermic rate of the composite paste. However, the test results have shown that the samples with B-doped MgO have a lower exothermic rate. It has been reported that borate could be used as a set retarder in cement [16,17]. The complexation of $B(OH)^{4-}$ could decrease the concentration of Ca^{2+} and, therefore, suppress the formation of the C-S-H nucleus and lower the exothermic rate. It is well accepted that the rate of hydration during the deceleration period is controlled by the diffusion process [18, 19]. A higher hydration rate before the deceleration period supports the formation of high-density C-S-H, which could limit the contact between cement particles and water, so the hydration rate decreases rapidly. Among the samples with the MgO incorporation, PM4B has the lowest hydration rate before the deceleration period, so the limitation on the contact between cement particles and water by the formed C-S-H is the lowest, which can sustain a higher hydration rate after the accelerating period shown in Figure 4a and the cumulative heat shown in Figure 4b.

Hydration products

The XRD patterns of pastes of the different ages are shown in Figure 5. There are no differences in the types of hydration products for the samples of the different ages, the only difference that can be seen is in the intensity of the diffraction peaks. Both the diffraction peaks of MgO and $Mg(OH)_2$ are shown in the patterns of the samples with MgO incorporation at 3 d, indicating that part of MgO has hydrated at 3 d, which is consistent with the results of the exothermic rate monitoring (the reason for the occurrence of the inflection point). The hydration of MgO in cement lasts for a long time. When the age reaches 28 d, part of the incorporated MgO has not hydrated, which would sustain the expansion of the sample afterward.

It is known that $Mg(OH)_2$ crystallises and grows on the MgO particles [20], the growth of $Mg(OH)_2$ can exert pressure on the matrices when it contacts

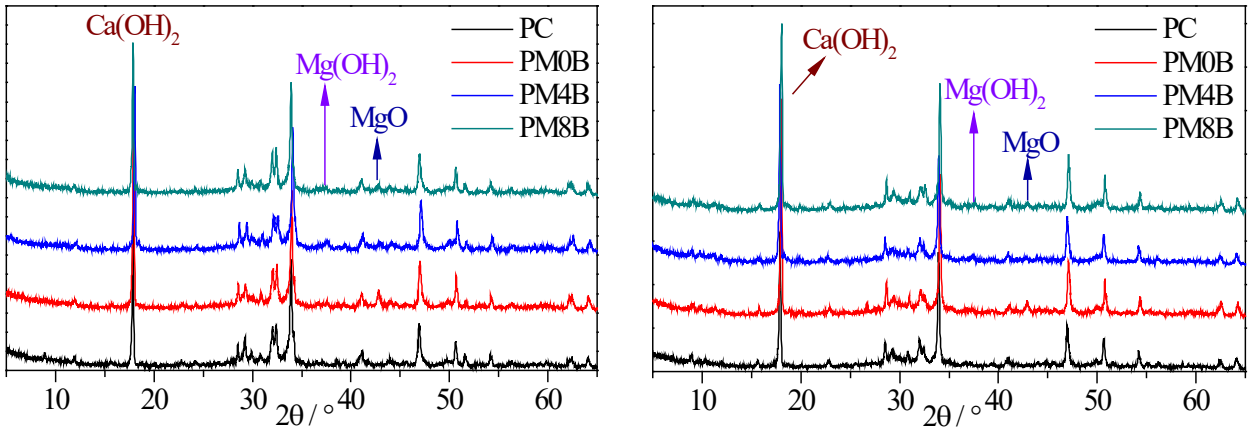

Figure 5. XRD patterns of the pastes at the different ages.

the wall of the pores nearby. Thus, the expansion behaviours of the cement pastes are determined by the amounts and characteristics of the formed $Mg(OH)_2$. As shown in Figure 5, there is no significant difference in the diffraction peaks of $Mg(OH)_2$. For a profound investigation of the composition of the hydration products, a thermogravimetric (TG) analysis was conducted to quantify the content of $Mg(OH)_2$ and $Ca(OH)_2$ formed at 28 d.

There are three obvious splitting endothermic peaks in the derivative thermogravimetry (DTG) curves. The peaks are located at 95 °C, 350 °C – 400 °C, and 400 °C – 470 °C, respectively. The endothermic peak at 95 °C characterises the thermal decomposition of ettringite and the loss of the free water, which has no practical reference on the compositions of the hydration products. The endothermic peak in the range of 350 °C – 400 °C corresponds to the thermal decomposition of $Mg(OH)_2$, and the endothermic peak in the range of 400 °C – 470 °C corresponds to the thermal decomposition of $Ca(OH)_2$. Therefore, it can be seen that there is no endothermic peak in the range of 350 °C – 400 °C in the curve of PC, indicating that no $Mg(OH)_2$ is formed. The content

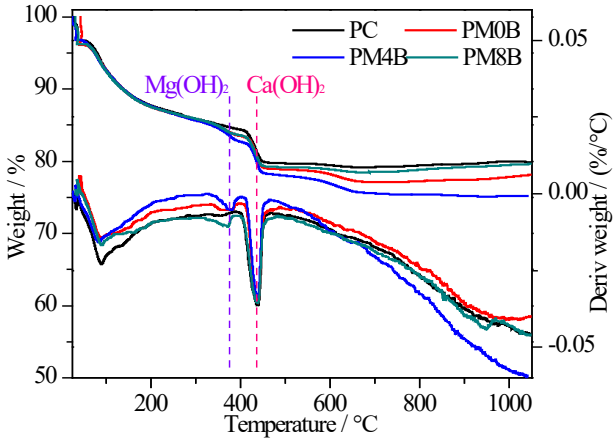

Figure 6. TG and DTG curves of the pastes at 28 d.

of $Mg(OH)_2$ and $Ca(OH)_2$ can be calculated based on Equation 2 and Equation 3.

$$Mass_{Mg(OH)_2} = \frac{58 \times massloss\left(400^{\circ}C - 350^{\circ}C\right)}{18} \quad (2)$$

$$Mass_{Ca(OH)_2} = \frac{74 \times massloss\left(470^{\circ}C - 400^{\circ}C\right)}{18} \quad (3)$$

It can be seen from Table 6 that the content of $Ca(OH)_2$ in PM0B is the highest in the samples with the MgO incorporation, meaning that the hydration degree of PM0B is the highest, the B dopant in the MgO suppresses the hydration of the cement pastes at 28 d. However, the B dopant in the MgO promotes the formation of $Mg(OH)_2$. Therefore, among the samples with the MgO incorporation, PM4B has the highest content of $Ma(OH)_2$ at 28 d. Then, it is clear that the maximum expansion of MM4B is attributed to the highest content of the $Mg(OH)_2$ formed in the paste.

Table 6. The mass fraction of $Mg(OH)_2$ and $Ca(OH)_2$ in the pastes at 28 d (%).

Hydration products	PM0B	PM4B	PM8B
$Mg(OH)_2$	4.06	6.35	4.16
$Ca(OH)_2$	18.71	18.67	17.92

Pore structures

Figure 7a and b show the cumulative pore volume and pore-size distribution results of the pastes at 28 d. The incorporation of MgO increases the porosity of the pastes. The porosity of PC is 0.188 $ml \cdot g^{-1}$, whereas the porosities of PM0B, PM4B, and PM8B are 0.191 $ml \cdot g^{-1}$, 0.197 $ml \cdot g^{-1}$, and 0.194 $ml \cdot g^{-1}$, respectively. In addition to the effect on the porosity, the pore distribution is also significantly influenced by the MgO incorporation. As shown in Figure 7b, the pores existing in the

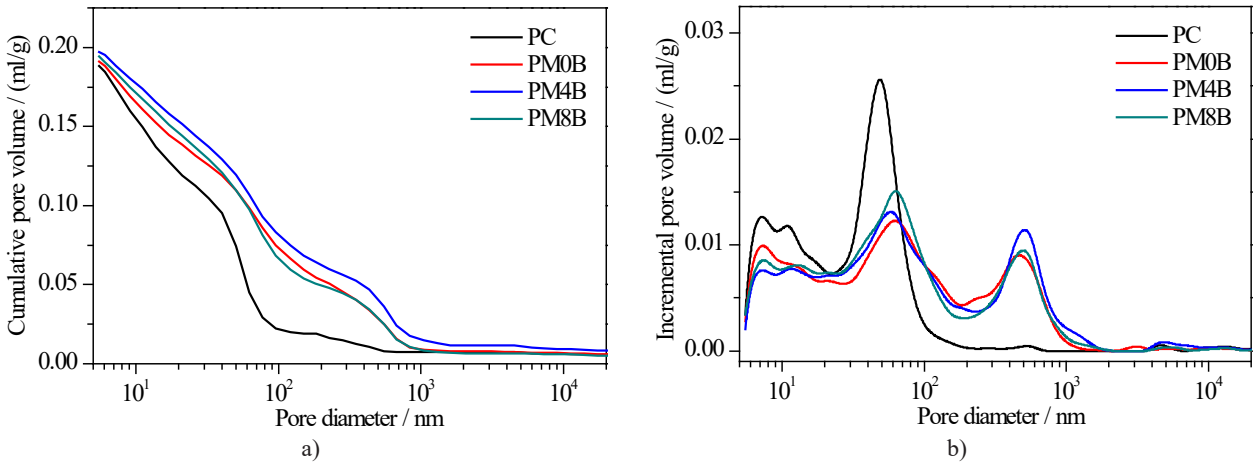

Figure 7. Pore structure of the pastes at 28 d.

pastes distribute in three intervals, namely gel pores (5 nm − 20 nm), micro pores (20 nm − 200 nm) and macro pores (200 nm − 2000 nm), respectively. The incorporation of MgO decreases the gel pores formed in the pastes; furthermore, M4B shows the highest decrease. The most probable pore size of the micro pores in PC is 49 nm, the incorporation of MgO enlarges the most probable pore size to more than 60 nm. Besides, the incorporation of MgO also decreases the micro pores formed in the pastes. The micro pores only appear in the pastes with the MgO incorporation, among these samples, the micro pores with a size between 200 nm and 2000 nm occur the most in PM4B.

On a nanoscale, C-S-H is presumed to be a gel-like phase which is comprised by many globules [21], the voids between the globules form the gel pores, so the volume of the gel pores is mainly determined by the content of the C-S-H. The incorporation of MgO decreases in the content of the cement and, therefore, leads to a decrease in the C-S-H content. Thus, the volume of the gel pores formed in the pastes with the MgO incorporations are less than that of plain cement pastes. Moreover, the $B(OH)^{4-}$ dissolved into the pore solution may also affect the C-S-H structure and alter the volume of the gel pores. With the hydration of the cement, the free water existing in the pastes is consumed, the room occupied by the water becomes empty, which leads to the formation of micro pores. The difference in the micro pores in the pastes with B-doped MgO results from the different hydration rates of the system.

The dissolution of MgO leads to the release of Mg^{2+} into the pore solution. As the pH of the pore solution of Portland cement is usually higher than 12, which is not conducive to the rapid diffusion of Mg^{2+}, the nucleus of $Mg(OH)_2$ preferentially forms near or on the surface of the MgO particles [22]. Afterward, with the hydration of MgO, the $Mg(OH)_2$ nucleus gradually grow. When the crystals come into contact with each other and the boundary movements are restricted, the growth pressure of the crystal will push the matrix away, resulting in the expansion [23]. The enlarged porosity and the appearance of the micro pores with a size between 200 nm − 2000 nm results from the growth of the $Mg(OH)_2$ crystals. The same trend in the change in the pore structures induced by the MgO incorporation was also reported by Mo [15] and Cao [20]. Among the samples with the MgO incorporation, PM4B shows the most significant porosity and the micro pores (between 200 nm − 2000 nm) at 28 d, which could be attributed to the highest $Ma(OH)_2$ content formed in the paste of PM4B.

Setting and mechanical properties

The initial setting time of the pastes with the different MgO incorporation is shown in Figure 8. The incorporation of pure MgO promotes the initial setting of the paste, which is advanced from 230 min to 200 min. It is consistent with the change in the exothermic rate of the cement paste at a very early age. The higher the exothermic rate, the faster the initial setting. Compared to

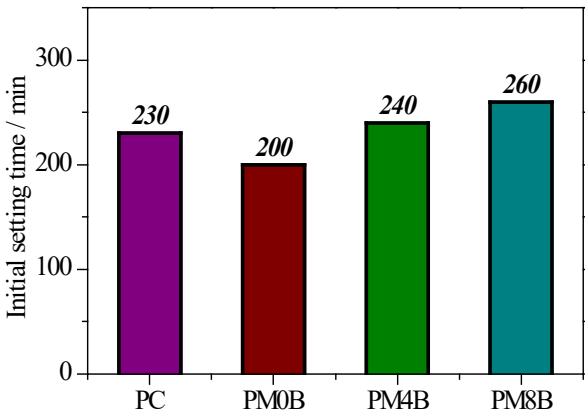

Figure 8. Initial setting time.

PM0B — with the incorporation of pure MgO, the B dopant in MgO delays the initial setting time of the paste; 4 % and 8 % the B dopant prolong the initial setting time by 40 min and 60 min, respectively. Identical to the change in the exothermic rate, the prolongation of the initial setting time is attributed to the complexation effect of $B(OH)_4^-$.

Figure 9 shows the compressive strength of the pastes with the different MgO incorporation at 3 d and 28 d. The incorporation of pure MgO doesn`t change the compressive strength. Whereas the incorporation of B-doped MgO significantly increases the compressive strength at 3 d, the incorporation of 4 % and 8 % B-doped MgO increase the compressive strength by 50 % compare to that of the sample without the B-doped MgO incorporation. This is in line with the effect of the B-doped MgO incorporation on the results of the cumulative heat at 3 d. With an increase in the curing age, the effect of the B-doped MgO incorporation on the compressive strength changes from promotion to reduction. As shown in Figure 9, compare to PC, the compressive strengths of PM0B, PM4B, and PM8B are reduced by 2 MPa, 6.7 MPa, and 12 MPa, respectively.

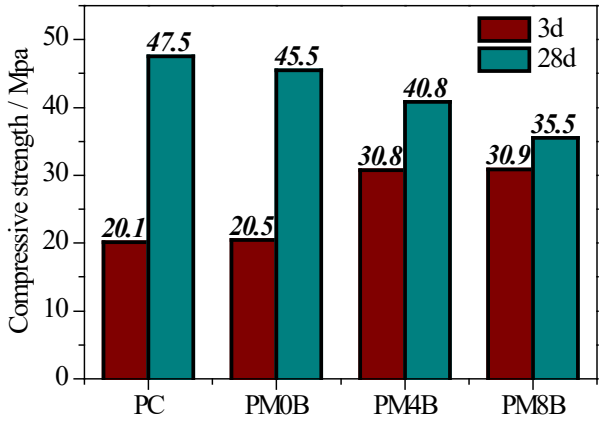

Figure 9. Compressive strength.

It had been reported that the MgO incorporation reduced the mechanical properties of Portland cement mortars at 28 d [24–26]. On the one hand, the MgO incorporation leads to the reduction of the C-S-H content, which can bond with the aggregate and, therefore, contribute a great deal to the mechanical properties of cement-based materials. On the other hand, the growth of $Mg(OH)_2$ (the hydrates of MgO) leads to cracks in the microstructures of the matrix and, therefore, increases the porosity of the pastes. The latter has been verified through the pore structure test in section "Pore structures". Based on the above, the reduction in the compressive strength of the pastes induced by the MgO incorporation is understandable.

CONCLUSION

Based on the above results and discussions, the following conclusions can be drawn:

The co-calcination of ($Mg(OH)_2$) and boric acid (H_3BO_3) at 800 °C changes the characteristics of the MgO crystals and their activity. With the increase in the dosage of B, the dimensions of the MgO crystals become smaller, and the reactive activity decreases.

The mortars with B-doped MgO show a higher final expansion rate than that of pure MgO. The dosage of B has a significant effect on the expansion behaviour of the mortars. The higher the dosage, the lower the expansion speed at the early age and the higher the expansion rate in the late period.

The incorporation of B-doped MgO alters the cement pastes' hydration process. Compared to the samples with the pure MgO and the 8 % B-doped MgO incorporation, the 4 % B-doped MgO incorporation leads to the highest cumulative heat at 28 d. Besides, the content of $Mg(OH)_2$ formed in the samples with the 4 % B-doped MgO is the highest, and the porosity of the samples is the highest compared to that of the others.

The initial setting time of cement pastes is delayed by the B doped-MgO incorporation. The higher the dosage of B, the longer the initial setting time. The incorporation also affects the mechanical properties of the cement pastes. For example, the B-doped MgO incorporation increases the compressive strength of the cement pastes at 3 d, but significantly decreases it at 28 d.

Acknowledgment

The authors would like to acknowledge the financial support of the fundamental research project of Qinghai Province (Grant No. 2022-ZJ-980Q) and the Youth Science Research Fund Project of Qinghai University (Grant No. 2020-QGY-7).

REFERENCES

1. Yan P. Y., Han J. G., Cao F. Z., Zhou Y. Q. (2018): The influencing factors of property and quality control of shrinkage-compensating concrete. *Construction technology, 47*(16), 97–99. doi:10.7672 /sgjs2018160097
2. Mo L. W., Deng M., Tang M.S. (2010): Effects of calcination condition on expansion property of MgO-type expansive agent used in cement-based materials. *Cement and Concrete Research, 40*, 437–446. doi:10.1016/j.cemconres.2009.09.025
3. Cao F. Z., Yan P. Y. (2017): Morphologies and performances of hydration products of expansive agents. *Journal of Chinese Electron Microscopy Society, 36*(2), 187–193. doi:10.3969 /j.issn.1000-6281.2017.02.015
4. Temiz H., Kantarci F., Inceer, Emin M. (2015): Influence of blast-furnace slag on behaviour of dolomite used as a

raw material of MgO-type expansive agent. *Construction and Building materials, 94*, 528–535. doi:10.1016/j.conbuildmat.2015.07.059
5. Xu L., Deng M. (2005): Dolomite used as raw material to produce MgO-based expansive agent. *Cement and Concrete Research, 35*, 1480–1485. doi: 10.1016/j.cemconres.2004.09.026
6. Gao P., Lu X., Jin S., Zhang H., Guo C. (2008): Using a new composite expansive material to decrease deformation and fracture of concrete. *Materials Letters, 62*, 106–108. doi:10.1016/j.matlet.2007.04.091
7. Gao P., Lu X., Geng F., Li X., Hou J., Hui J., Shi N. (2008): Production of MgO-type expansive agent in dam concrete by use of industrial by-products. *Building and Environment, 43*, 453–457. doi:10.1016/j.buildenv.2007.01.037
8. Fu Y., Zhong H. (2010): Research progress of production magnesium hydroxide from salt lake. *Journal of Salt and Chemical industry, 39*(01), 49-52.
9. Tan Y. S., Yu H. F., Li Y., Wu C. Y., Dong J. M., Wen J. (2014): Magnesium potassium phosphate cement prepared by the byproduct of magnesium oxide after producing Li2CO3 from salt lakes. *Ceramics International, 40*, 13543–13551. doi:10.1016/j.ceramint.2014.05.063
10. Dong J. M., Yu H. F., Xiao X. Y., Li Y., Wu C. Y., Wen J., Tan, Tan Y. S., Chang C. G., Zheng W. X. (2016): Effects of calcination temperature of boron-containing magnesium oxide raw materials on properties of magnesium phosphate cement as a biomaterial. *Journal of Wuhan University of Technology-Mater, 31*(3), 671–676. doi:10.1007/s11595-016-1427-3
11. Li Y., Dong J. M., Xiao X. Y., Zheng W. X., Wen J., Chang C. G. (2020): Green preparation of magnesia and magnesium phosphate cement by utilizing common elements in salt lake as sintering aid. *Journal of Salt Lake Research, 28*(02), 15–25. doi:10. 12119/j.yhyj.202002002
12. Wu C. Y., Chen C., Zhang H. F., Tan Y. S., Yu H. F. (2018): Preparation of magnesium oxysulfate cement using magnesium-rich byproducts from the production of lithium carbonate from salt lakes. *Construction and Building Materials, 172*, 597-607. doi:10.1016/j.conbuildmat.2018.04.005
13. Miao M., Wu C. Y., Tan Y. S., Yu H. F. (2020): Mechanistic study of the effects of magnesia reactivity on setting and hardening of basic magnesium sulfate cement. *Journal of Advanced Concrete Technology, 18*, 678–688. doi:10.3151/JACT.18.678
14. Juilland P., Gallucci E., Flatt R., Scrivener K. (2010): Dissolution theory applied to the induction period in alite hydration. *Cement and Concrete Research, 40*, 831–844. doi:10.1016/j.cemconres.2010.01.012
15. Mo L. W., Fang J. W., Hou W. H., Ji X. K., Yang J. B,, Fan T. T., Wang H. L. (2019). Synergetic effects of curing temperature and hydration reactivity of MgO expansive agents on their hydration and expansion behaviours in cement pastes. *Construction and Building Materials, 207,* 206-217. doi:10.1016/j.conbuildmat.2019.02.150
16. Kula I., Olgun A., Sevinc V., Erdogan Y. (2002): An investigation on the use of tincal ore waste, fly ash, and coal bottom ash as Portland cement replacement materials. *Cement and Concrete Research, 32*, 227–232. doi:10.1016/s0008-8846(01)00661-5
17. Bullerjahn F., Zajac M., Skocek J., Ben Haha M. (2019): The role of boron during the early hydration of belite ye'elimite ferrite cements. *Construction and Building Materials, 215*, 252-263. doi:10.1016/j.cemconres.2010.09.011
18. Bullard J. W., Jennings H. M., Livingston R. A., Nonat A., Scherer G. W., Schweitzer J. S., Scrivener K. L., Thomas J. J. (2011): Mechanisms of cement hydration. *Cement and Concrete Research, 41*, 1208–1223. doi:10.1016/j.cemconres.2010.09.011
19. Kong X M., Lu Z. C., Zhang C. Y. (2017): Recent development on understanding cement hydration mechanism and effects of chemical admixtures on cement hydration. *Journal of the Chinese Ceramic Society, 45*(2), 274–281. doi:10.14062/j.issn.0454-5648.2017.02.15
20. Cao F. Z., Miao M., Yan P. Y. (2018): Hydration characteristics and expansive mechanism of MgO expansive agents. *Construction and Building Materials, 183*, 234–242. doi:10.1016/j.conbuildmat.2018.06.164
21. Zhang Q., Ye G., Koenders E. (2013): Investigation of the structure of heated Portland cement paste by using various techniques. *Construction and Building Materials, 38*, 1040–1050. doi: 10.1016/j.conbuildmat.2012.09.071
22. Deng M., Cui X. H., Liu Y. Z., Tang M. S. (1990): expansive mechanism of magnesia as an additive of cement. *Journal of Nanjing Institute of Chemical Technology, 12*(4), 1-11.
23. Chatterji S. (1995): Mechanism of expansion of concrete due to the presence of dead burnt CaO and MgO. *Cement and Concrete Research, 25*(1), 51–56. doi:10.1016/0008-8846(94)00111-B
24. Ding W., Tan K., Liu L., Tang L., Zhao C., He Y. (2016): Utilization of light calcined magnesite tailings to compensate the autogenous shrinkage of steam-cured cement paste. *Advance in Cement Research, 28*(10), 675–686. doi:10.1680/jadcr.16.00016
25. Mo L. W., Liu M., Al-Tabbaa A., Deng M., Lau W. Y., (2015): Deformation and mechanical properties of quaternary blended cements containing ground granulated blast furnace slag, fly ash and magnesia. *Cement and Concrete Research, 71*, 7–13. doi:10.1016/j.cemconres.2015.01.018
26. Cao F. Z., Liu Y., Yan P. Y. (2021): Properties and mechanism of the compound MgO expansive agent (CMEA) produced by calcining the mixture of dolomite and serpentine tailings. *Construction and Building Materials, 27*, 122331. doi:10.1016/j.conbuildmat.2021.122331